Radical Cations

DOI: 10.1002/ange.200501132

Phenoxyl Radicals Hydrogen-Bonded to Imidazolium: Analogues of Tyrosyl D· of Photosystem II: High-Field EPR and DFT Studies**

Laurent Benisvy, Robert Bittl, Eberhard Bothe, C. David Garner, Jonathan McMaster, Stephanie Ross, Christian Teutloff, and Frank Neese**

Tyrosyl radicals play a crucial role in many biological systems.[1] The remarkably stable tyrosyl radical, Tyr_D· in photosystem II (PSII)[2] is suggested to be hydrogen-bonded to an imidazol(ium) proton from a nearby histidine residue[3] (His 190 in higher plants; His 189 in cyanobacteria). Oxidation of Tyr_D to Tyr_D· probably proceeds via proton-coupled electron transfer (PCET) with migration of the phenoxyl proton to the imidazole group of the adjacent histidine.[4] Production of chemical analogues of Tyr_D· is of much current theoretical and experimental interest. Three recent studies have reported the oxidation of an α-alkylaminophenol derivative by a quasireversible PCET process, to form a phenoxyl radical hydrogen-bonded to an alkylammonium center.[5]

We have reported the synthesis and characterization of (**1**–**3**)H,[6] each of which has an intramolecular hydrogen bond involving the phenolic proton and an imidazole nitrogen atom. (**1**–**3**)H undergo a reversible, one-electron oxidation to form the corresponding radical cation, $[(\mathbf{1}–\mathbf{3})H]^{\bullet+}$. The oxidation of (**1**–**3**)H (see Scheme 1) could occur either by

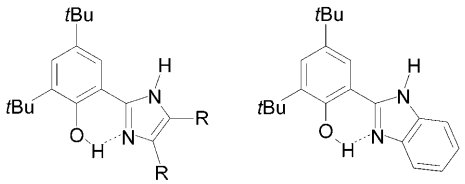

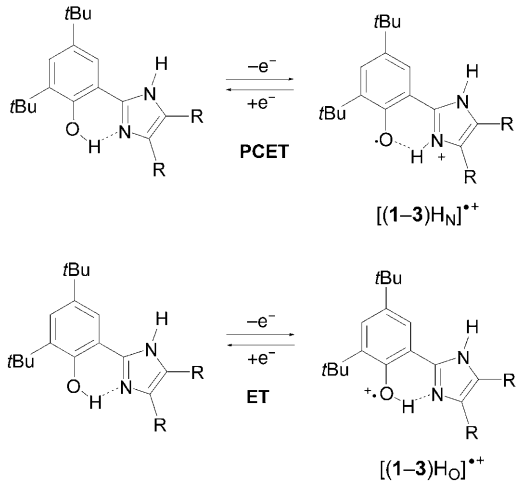

Scheme 1. Possible mechanisms for the oxidation of (**1**–**3**)H to $[(\mathbf{1}–\mathbf{3})H]^{\bullet+}$.

PCET to produce an R–O···H–N^+ arrangement (designated $[(\mathbf{1}–\mathbf{3})H_N]^{\bullet+}$) or by electron transfer (ET) to produce an R–$O^{+\bullet}$–H···N arrangement (designated as $[(\mathbf{1}–\mathbf{3})H_O]^{\bullet+}$). Herein, we report the results of high-field EPR studies and DFT calculations that provide a definitive interpretation of the geometric and electronic structure of these $[(\mathbf{1}–\mathbf{3})H]^{\bullet+}$ radical cations.

The X-band EPR spectra of $[(\mathbf{1}–\mathbf{3})H]^{\bullet+}$ in CH_2Cl_2 at 77 K each consist of a single isotropic signal, centered at $g \approx 2.004$ with a linewidth of about 10 G and no discernible hyperfine splitting.[6] The absence of hyperfine splitting and the unresolved *g*-tensor anisotropy preclude any geometric and electronic structural information being obtained from the X-band EPR spectra alone. The lack of resolved proton hyperfine splittings may be taken as evidence for the presence of the $[(\mathbf{1}–\mathbf{3})H_N]^{\bullet+}$ forms of the radicals. However, a more positive experimental proof for this conjecture is required and is provided by high-field EPR. W-band (94.0 GHz) high-field EPR spectra, recorded for electrochemically generated $[(\mathbf{1}–\mathbf{3})H]^{\bullet+}$ in CH_2Cl_2 solution (1 mM) at 80 K (Figure 1 and Supporting Information) show three well-resolved *g* values; each spectrum was simulated successfully with $g_x = 2.0063$–2.0067, $g_y = 2.0043$, and $g_z = 2.0022/3$ (Table 1).

Density functional calculations were performed to interpret the W-band EPR spectra of $[(\mathbf{1}–\mathbf{3})H]^{\bullet+}$ and to investigate whether these data discriminate between the possible structures $[(\mathbf{1}–\mathbf{3})H_N]^{\bullet+}$ and $[(\mathbf{1}–\mathbf{3})H_O]^{\bullet+}$ (Scheme 1). As a calibration, the DFT calculations were performed initially for (**1**–**3**)H. In each case, the calculated structural parameters were in good agreement with the corresponding data obtained by X-ray crystallography;[6] the value of each bond length was reproduced to an accuracy of not worse than ±0.03 Å (see Supporting Information). For the corresponding $[(\mathbf{1}–\mathbf{3})H]^{\bullet+}(g)$ radical cations, DFT calculations were performed for the two forms $[(\mathbf{1}–\mathbf{3})H_N]^{\bullet+}$ and $[(\mathbf{1}–\mathbf{3})H_O]^{\bullet+}$, and in each

[*] Dr. L. Benisvy, Dr. E. Bothe, PD Dr. F. Neese
Max-Planck-Institut für Bioanorganische Chemie
Stiftstrasse 34–46, 45470 Mülheim an der Ruhr (Germany)
Fax: (+49) 208-306-3951
E-mail: benisvy@mpi-muelheim.mpg.de
neese@mpi-muelheim.mpg.de
Prof. C. D. Garner, Dr. J. McMaster, S. Ross
School of Chemistry
The University of Nottingham
University Park, Nottingham, NG72RD (UK)
Prof. Dr. R. Bittl, Dr. C. Teutloff
Institut für Experimentalphysik
Freie Universität Berlin
Arnimallee 14, 14195 Berlin (Germany)

[**] The authors thank Miss Petra Höfer for technical assistance and Dr. Sebastian Sinnecker for help with the electronic structure calculations. This work has been supported by Deutsche Forschungsgemeinschaft (Sfb 498 TP C5 and SPP 1137) and the Engineering and Physical Sciences Research Council (UK) (GR/R50325/01).

Supporting information for this article is available on the WWW under http://www.angewandte.org or from the author.

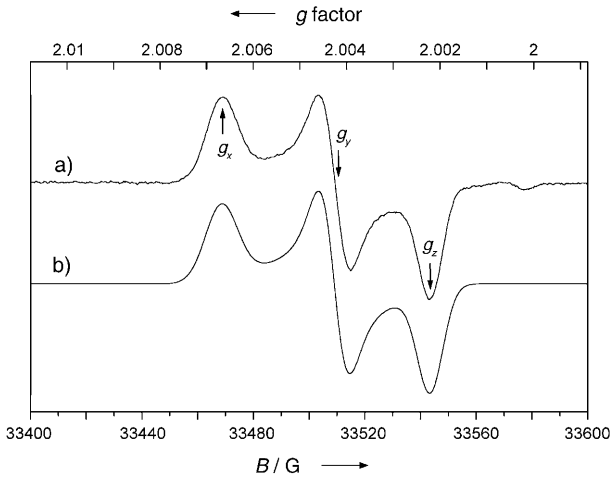

Figure 1. W-band EPR spectra of $[\mathbf{3}H]^{\bullet+}$. a) Spectrum recorded for electrochemically generated $[\mathbf{3}H]^{\bullet+}$ (1 mM) in CH_2Cl_2 at 80 K. b) Spectrum simulated by using the parameters listed in Table 1.

Table 1: Comparison of the experimental W-band g values obtained for $[(\mathbf{1}–\mathbf{3})H]^{\bullet+}$ and those calculated by DFT for $[(\mathbf{1}–\mathbf{3})H_O]^{\bullet+}$ and $[(\mathbf{1}–\mathbf{3})H_N]^{\bullet+}$.

Radical		g_x	g_y	g_z	g_{iso}
$[\mathbf{1}H]^{\bullet+}$	exptl	2.0065	2.0043	2.0022	2.0043
$[\mathbf{1}H_N]^{\bullet+}$	calcd	2.0066	2.0043	2.0023	2.0044
$[\mathbf{1}H_O]^{\bullet+}$	calcd	2.0034	2.0030	2.0023	2.0029
$[\mathbf{2}H]^{\bullet+}$	exptl	2.0063	2.0043	2.0023	2.0043
$[\mathbf{2}H_N]^{\bullet+}$	calcd	2.0064	2.0042	2.0023	2.0043
$[\mathbf{2}H_O]^{\bullet+}$	calcd	2.0036	2.0031	2.0024	2.0030
$[\mathbf{3}H]^{\bullet+}$	exptl	2.0067	2.0043	2.0022	2.0044
$[\mathbf{3}H_N]^{\bullet+}$	calcd	2.0068	2.0043	2.0023	2.0044
$[\mathbf{3}H_O]^{\bullet+}$	calcd	2.0044	2.0038	2.0022	2.0035

case convergence to a distinct energy minimum occurred. The difference in energy of the two forms of $[(\mathbf{1}–\mathbf{3})H]^{\bullet+}(g)$, $\Delta E = [E([(\mathbf{1}–\mathbf{3})H_N]^{\bullet+}) - E([(\mathbf{1}–\mathbf{3})H_O]^{\bullet+})]$, is calculated as -4.8, $+7.7$, and $-26.4\ kJ\,mol^{-1}$ for **1**H, **2**H, and **3**H, respectively. These results suggest that $[(\mathbf{1}–\mathbf{3})H_N]^{\bullet+}$ (the proton-transferred species) is favored for $[\mathbf{1}H]^{\bullet+}(g)$ and $[\mathbf{3}H]^{\bullet+}(g)$, but not for $[\mathbf{2}H]^{\bullet+}(g)$.

The bond lengths calculated for the geometry-optimized structures of $[(\mathbf{1}–\mathbf{3})H_N]^{\bullet+}$ and $[(\mathbf{1}–\mathbf{3})H_O]^{\bullet+}$ are listed in Table SI2. Each optimized structure involves an intramolecular hydrogen bond: for $[(\mathbf{1}–\mathbf{3})H_O]^{\bullet+}$, the H···N distances are calculated as 1.600 (**1**H), 1.623 (**2**H), and 1.435 Å (**3**H); for $[(\mathbf{1}–\mathbf{3})H_N]^{\bullet+}$, the O···H distances are calculated as 1.832 (**1**H), 1.781 (**2**H), and 1.867 Å (**3**H; see Supporting Information).

The g-tensor parameters calculated by DFT for $[(\mathbf{1}–\mathbf{3})H_N]^{\bullet+}$ and $[(\mathbf{1}–\mathbf{3})H_O]^{\bullet+}$ are compared with those observed experimentally in Table 1. In each case, the g values calculated for $[(\mathbf{1}–\mathbf{3})H_N]^{\bullet+}$ correspond very closely (within 100 ppm) to those observed experimentally; however, this is not true for the g values calculated for $[(\mathbf{1}–\mathbf{3})H_O]^{\bullet+}$: in particular, each g_x is calculated to be significantly lower (2000–3000 ppm) than the experimental value. Moreover, the W-band EPR spectrum of each $[(\mathbf{1}–\mathbf{3})H]^{\bullet+}$ is consistent with the presence of only a single species. Therefore, we conclude that all of the radical cations $[(\mathbf{1}–\mathbf{3})H]^{\bullet+}$ in CH_2Cl_2 solution at 80 K are present as $[(\mathbf{1}–\mathbf{3})H_N]^{\bullet+}$. Consequently, the slight energetic preference ($+7.7\ kJ\,mol^{-1}$) for $[\mathbf{2}H_O]^{\bullet+}(g)$ given by the DFT calculations is considered to be in error.

The nature of the singly occupied molecular orbital (SOMO) and the corresponding unpaired spin-density distribution were analyzed for both $[(\mathbf{1}–\mathbf{3})H_N]^{\bullet+}$ and $[(\mathbf{1}–\mathbf{3})H_O]^{\bullet+}$ (Figure 2 and Supporting Information). Each $[(\mathbf{1}–\mathbf{3})H_O]^{\bullet+}$

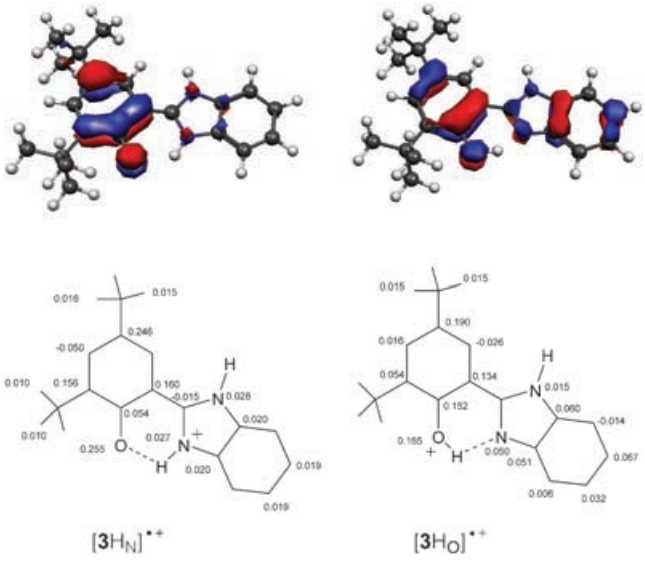

Figure 2. SOMO orbitals (top) and the spin populations (bottom) for $[\mathbf{3}H_N]^{\bullet+}$ and $[\mathbf{3}H_O]^{\bullet+}$.

involves a SOMO that extends over the phenol and imidazole rings with phenol/imidazole distributions of the unpaired spin population of approximately 70:30, 40:60, and 25:75 for $[\mathbf{3}H_O]^{\bullet+}$, $[\mathbf{1}H_O]^{\bullet+}$, and $[\mathbf{2}H_O]^{\bullet+}$, respectively. In contrast, the SOMO of each $[(\mathbf{1}–\mathbf{3})H_N]^{\bullet+}$ is localized primarily on the phenol ring, and the phenol/imidazole distribution of the unpaired spin population is approximately 90:10, 80:20, and 65:35 for $[\mathbf{3}H_N]^{\bullet+}$, $[\mathbf{1}H_N]^{\bullet+}$, and $[\mathbf{2}H_N]^{\bullet+}$, respectively. Thus, these calculations indicate that the electronic structure of $[\mathbf{3}H_N]^{\bullet+}$ is essentially that of a phenoxyl radical hydrogen-bonded to an imidazolium cation.

For the phenol ring of each $[(\mathbf{1}–\mathbf{3})H_N]^{\bullet+}$, the typical[5b,7] pattern of an alternating spin-density distribution is obtained with a significant amount of positive spin population located at the O, C_{ortho}, and C_{para} atoms (Figure 2 and Supporting Information). Also, there is a positive spin population at the phenolic carbon atom that is indicative of a redistribution of the spin density from that of an isolated phenoxyl radical and is attributed to hydrogen-bond formation.[7] The length of the C–O bond is calculated (Table SI2) to be significantly longer in $[(\mathbf{1}–\mathbf{3})H_O]^{\bullet+}$ (1.332 (**1**H), 1.343 (**2**H), and 1.307 Å (**3**H)) than in $[(\mathbf{1}–\mathbf{3})H_N]^{\bullet+}$ (1.265 (**1**H), 1.270 (**2**H), and 1.261 Å (**3**H)). The latter values are in excellent agreement with: 1) the length of the C–O bond of $\mathbf{1}^{\bullet}$ (1.264(5) Å) in the Cu^{II}–phenoxyl radical complex $[Cu(\mathbf{1}^{\bullet})(\mathbf{1})](BF_4)$[6a,b] and 2) those calculated (1.26–1.27 Å) for the C–O bond of a phenoxyl radical hydrogen-bonded to an imidazolium group.[7]

The above analysis of the g tensors has illustrated that this approach represents a powerful tool for determining the nature of a phenoxyl radical. Theoretical[7,8] and experimental studies[4,5b,9] have indicated that hydrogen bonding to a phenoxyl (or tyrosyl) radical results in a considerable lowering of the g_x value but leaves g_y and g_z essentially unaffected. The g_x values observed for each $[(\mathbf{1}\text{–}\mathbf{3})H_N]^{\bullet+}$ (2.0065–2.0067, Table 1) are very similar to those observed for hydrogen-bonded tyrosyl radicals; for example, for γ-irradiated crystals of tyrosine·HCl, $g_x = 2.0067$;[10] $Tyr_D^{\bullet}$ of PSII, $g_x = 2.00643$ (radical generated at cryogenic temperature)[4] and $g_x = 2.00756$ (radical generated at physiological temperature);[11] $Tyr^{\bullet}$ of HSV1 RNR: $g_x = 2.0076$[12] and hydrogen-bonded phenoxyl radical compounds (g_x ranging from 2.0061 to 2.0066).[5b] These g_x values are significantly lower than those observed for non-hydrogen-bonded tyrosyl radicals; for example, $Tyr^{\bullet}$ of *E. coli* RNR, $g_x = 2.0087$,[9] or of *S. typhimurium* RNR,[13] $g_x = 2.0089$.

Theoretical studies of the g tensors of aromatic free radicals[14] indicate that variations in the g_x value of a phenoxyl radical may be understood as arising from a combination of two effects: 1) changes in the unpaired spin population at the oxygen atom, the constituent atom with the largest spin–orbit coupling constant; and 2) changes in the relative energies of two oxygen-based orbitals, the out-of-plane p_z orbital, which makes a significant contribution to the SOMO of a phenoxyl radical, and the in-plane p_y lone pair orbital, the contribution of which to the g shift arises as a result of spin–orbit coupling with the electron in the SOMO. This latter effect produces a magnetic moment along the C–O axis that increases the value of g_x. Formation of an in-plane hydrogen bond stabilizes the p_y lone pair, increases the energy difference between this orbital and the SOMO, and results in less effective spin–orbit coupling and a decrease in the g_x value (vide infra). In this respect, the species $[(\mathbf{1}\text{–}\mathbf{3})H_O]^{\bullet+}$ represent extreme cases in which the p_y lone pair is directly involved in the O–H bond and therefore, is not involved in efficient spin–orbit coupling with the SOMO, which explains the very low g_x values calculated for these species. For the $[(\mathbf{1}\text{–}\mathbf{3})H_N]^{\bullet+}$ radical cations, the DFT calculations indicate that the strength of the hydrogen bond increases across this series, that is, the O···HN distance decreases (1.867, 1.832, and 1.781 Å, respectively; see Supporting Information) and leads to a decreased g_x value. For these $[(\mathbf{1}\text{–}\mathbf{3})H_N]^{\bullet+}$ systems, in addition to the effect of hydrogen bonding on the g_x value, the extent of the delocalization of the unpaired electron onto the imidazole ring must be considered. Across this series, the unpaired spin population at the oxygen atom ($\rho(O) = 0.255$, 0.230, and 0.189, respectively; see Figure 2 and Supporting Information) decreases as a result of the increased delocalization of the unpaired spin density onto the imidazole ring (vide infra), and this also will lead to a decrease in the g_x value. Thus, these two effects operate in the same sense, consistent with the relative magnitudes of the g_x values of $[\mathbf{3}H_N]^{\bullet+}$ (2.0067), $[\mathbf{1}H_N]^{\bullet+}$ (2.0065), and $[\mathbf{2}H_N]^{\bullet+}$ (2.0063).

In conclusion, we have demonstrated that the one-electron oxidation of (**1**–**3**)H occurs by a PCET mechanism and produces the corresponding $[(\mathbf{1}\text{–}\mathbf{3})H_N]^{\bullet+}$; that is, a phenoxyl radical hydrogen-bonded to an imidazolium cation. The resolution of the principal g values by W-band EPR spectroscopy and the interpretation of these data by DFT calculations were essential in determining the nature of the $[(\mathbf{1}\text{–}\mathbf{3})H]^{\bullet+}$ radical cations. Furthermore, the DFT calculations provided valuable insight into the electronic structure of these species. The g_x value of the $[(\mathbf{1}\text{–}\mathbf{3})H_N]^{\bullet+}$ radical cations is lower than that of a simple phenoxyl radical owing to delocalization of the unpaired spin and orbital-stabilization effects, both of which are directly related to the formation of an O···HN hydrogen bond. These $[(\mathbf{1}\text{–}\mathbf{3})H_N]^{\bullet+}$ radical cations, notably $[\mathbf{3}H_N]^{\bullet+}$, represent valuable chemical analogues of $Tyr_D^{\bullet}$ in PSII, and further spectroscopic and theoretical studies of these species are currently being undertaken in our laboratories.

Experimental Section

Each radical cation was generated electrochemically by controlled potential coulometry with a platinum-grid working electrode, an $Ag/AgNO_3$ reference electrode, and a platinum brush in a counter electrode compartment. Each experiment was performed under dinitrogen at −25 °C with the compound (1 mM) in degassed CH_2Cl_2 containing $[n\mathrm{Bu_4N}](BF_4)$ (0.2 M) as background electrolyte. The solution was transferred under exclusion of dioxygen into a W-band quartz tube (inner diameter 0.7 mm, length 3 cm) with a microsyringe. Each tube was inserted into a cryovial which was immediately frozen and stored in liquid nitrogen.

All calculations were performed with the ORCA program.[15] Geometry optimizations were performed in redundant internal coordinates by using the pure density functional[16] BP[17] method with the TZVP[18] basis set on all atoms. For both the geometry optimization of the radical species and the g-tensor calculation, the CH_2Cl_2 solvent ($\varepsilon = 9.08$) was simulated by the COSMO dielectric continuum approach.[19] The B3LYP[20] hybrid DFT method, together with the EPR-II[21] basis set, was employed for the calculation of the magnetic properties at the optimized geometries of the radical species. Molecular g tensors were calculated by the coupled-perturbed Kohn–Sham method[22] and the multicenter, spin–orbit mean-field[23] (SOMF) spin-orbit coupling operator in the resolution-of-the-identity approximation.[24]

W-band (94 GHz) spectra were recorded on a Bruker Elexsys E680 spectrometer at 80 K with a microwave power of 0.32 μW, 5 G field modulation amplitude at 10 kHz modulation frequency, and a lock-in time constant of 82 ms. The magnetic field was calibrated against a LiLiF g standard[25] at microwave frequencies measured by the integrated frequency counter; all spectra were normalized to 94.0 GHz. The simulated spectra and the associated parameters were obtained with Bruker Simfonia software.

Received: March 30, 2005
Published online: July 22, 2005

Keywords: density functional calculations · electronic structure · EPR spectroscopy · hydrogen bonds · radical ions

[1] a) J. Stubbe, W. A. van der Donk, *Chem. Rev.* **1998**, *98*, 705–762; b) J. Stubbe, D. G. Nocera, C. S. Yee, M. C. Y. Chang, *Chem. Rev.* **2003**, *103*, 2167–2201.

[2] a) G. T. Babcock, M. Espe, C. Hoganson, N. Lydakis-Simantiris, J. McCracken, W. Shi, S. Styring, C. Tommos, K. Warncke, *Acta Chem. Scand.* **1997**, *51*, 533–540; b) G. M. Ananyey, I. Sakiyan, B. A. Diner, G. C. Dismukes, *Biochemistry* **2002**, *41*, 974–980; c) A. W. Rutherford, A. Boussac, P. Faller, *Biochim. Biophys. Acta* **2004**, *1655*, 222–230.

[3] K. A. Campell, J. M. Peloquin, B. A. Diner, X.-S. Tang, D. A. Chisholm, R. D. Britt, *J. Am. Chem. Soc.* **1997**, *119*, 4787 – 4788.
[4] P. Faller, C. Goussias, A. W. Rutherford, S. Un, *Proc. Natl. Acad. Sci. USA* **2003**, *100*, 8732 – 8735.
[5] a) T. Maki, Y. Araki, Y. Ishida, O. Onomura, Y. Matsumura, *J. Am. Chem. Soc.* **2001**, *123*, 3371 – 3372; b) F. Thomas, O. Jarjayes, H. Jamet, S. Hamman, E. Saint-Aman, C. Duboc, J.-L. Pierre, *Angew. Chem.* **2004**, *116*, 604 – 607; *Angew. Chem. Int. Ed.* **2004**, *43*, 594 – 597; c) I. J. Rhile, J. M. Mayer, *J. Am. Chem. Soc.* **2004**, *126*, 12718 – 12719; d) I. J. Rhile, J. M. Mayer, *Angew. Chem.* **2005**, *117*, 1624 – 1625; *Angew. Chem. Int. Ed.* **2005**, *44*, 1598 – 1599.
[6] a) L. Benisvy, A. J. Blake, D. Collison, E. S. Davies, C. D. Garner, E. J. L. McInnes, J. McMaster, G. Whittaker, C. Wilson, *Chem. Commun.* **2001**, 1824 – 1825; b) L. Benisvy, A. J. Blake, D. Collison, E. S. Davies, C. D. Garner, E. J. L. McInnes, J. McMaster, G. Whittaker, C. Wilson, *Dalton Trans.* **2003**, 1975 – 1985; c) L. Benisvy, E. Bill, A. J. Blake, D. Collison, E. S. Davies, C. D. Garner, C. I. Guindy, E. J. L. McInnes, G. McArdle, J. McMaster, C. Wilson, J. Wolowska, *Dalton Trans.* **2004**, 3647 – 3653; d) L. Benisvy, E. Bill, A. J. Blake, D. Collison, E. S. Davies, C. D. Garner, E. J. L. McInnes, J. McMaster, S. Ross, C. Wilson, unpublished results; e) L. Benisvy, PhD Thesis, University of Nottingham, Nottingham, UK, **2001**.
[7] P. J. O'Malley, *J. Am. Chem. Soc.* **1998**, *120*, 11732 – 11737.
[8] a) J. R. Asher, N. L. Doltsinis, M. Kaupp, *J. Am. Chem. Soc.* **2004**, *126*, 9854 – 9861; b) M. Kaupp, T. Gress, R. Reviakine, O. L. Malkina, V. G. Malkin, *J. Phys. Chem. B* **2003**, *107*, 331 – 337; c) M. Engström, F. Himo, A. Gräslund, B. Minaev, O. Vahtras, H. Ågren, *J. Phys. Chem. A* **2000**, 104, 5149 – 5153.
[9] S. Un, M. Atta, M. Fontecave, A. W. Rutherford, *J. Am. Chem. Soc.* **1995**, *117*, 10713 – 10719.
[10] E. L. Fasanella, W. Gordy, *Proc. Natl. Acad. Sci. USA* **1969**, *62*, 299 – 304.
[11] P. Dorlet, A. W. Rutherford, S. Un, *Biochemistry* **2000**, *39*, 7826 – 7834.
[12] P. J. van Dam, J.-P. Willems, P. P. Schmidt, S. Pötsch, A.-L. Barra, W. R. Hagen, B. M. Hoffman, K. K. Andersson, A. Gräslund, *J. Am. Chem. Soc.* **1998**, *120*, 5080 – 5085.
[13] P. Allard, A.-L. Barra, K. K. Andersson, P. P. Schmidt, M. Atta, A. Gräslund, *J. Am. Chem. Soc.* **1996**, *118*, 895 – 896.
[14] a) A. J. Stone, *Mol. Phys.* **1963**, *6*, 509 – 515; b) A. J. Stone, *Mol. Phys.* **1964**, *7*, 311 – 316.
[15] F. Neese, ORCA, An ab initio, Density Functional and Semi-empirical Program Package, Version 2.4.13, Max-Planck-Institut für Bioanorganische Chemie, Mülheim an der Ruhr, Germany, **2004**.
[16] W. Koch, M. C. Holthausen, *A Chemist's Guide to Density Functional Theory*, Wiley-VCH, Weinheim, **2000**.
[17] a) A. D. Becke, *Phys. Rev. A* **1988**, 38, 3098 – 3100; b) J. P. Perdew, *Phys. Rev. B* **1986**, 33, 8822 – 8824.
[18] A. Schäfer, C. Huber, R. Ahlrichs, *J. Chem. Phys.* **1994**, *100*, 5829 – 5835.
[19] A. Klamt, G. Schüürmann, *J. Chem. Soc.*, *Perkin Trans.* 2 **1993**, 793 – 805.
[20] a) C. T. Lee, W. T. Yang, R. G. Parr, *Phys. Rev. B* **1988**, *37*, 785 – 789; b) A. D. Becke, *J. Chem. Phys.* **1993**, *98*, 5648 – 5652; c) P. J. Stephens, F. J. Devlin, C. F. Chabalowski, M. J. Frisch, *J. Phys. Chem.* **1994**, *98*, 11623 – 11627.
[21] V. Barone in *Recent Advances in Density Functional Methods* (Ed.: D. P. Chong), World Scientific Publishing, Singapore, **1996**.
[22] F. Neese, *J. Chem. Phys.* **2001**, *115*, 11080 – 11096.
[23] B. A. Hess, C. M. Marian, U. Wahlgren, O. Gropen, *Chem. Phys. Lett.* **1996**, *251*, 365 – 371.
[24] F. Neese, *J. Chem. Phys.* **2005**, *122*, 034107/1 – 13.
[25] A. Stesmans, G. van Gorp, *Rev. Sci. Instrum.* **1989**, *60* 2949 – 2952.

